Atomic Force Microscopy Study of Conducting Layered Transition Metal Ditellurides

Sung-Jin Kim*, So-Jung Park, Hoon-Jung Oh, Il Cheol Jeon†, and Sunae Song†

Department of Chemistry, Ewha Womans University, Seoul 120-750, Korea
†Department of Chemistry, Jeonbuk National University, Jeonbuk 560-756, Korea
Received August 26, 1994

Atomic force microscopy (AFM) images of two conducting layered transition-metal ditellurides, $TaTe_2$ and $Ta_{0.5}V_{0.5}Te_2$, were examined and their surface and bulk structural features were compared. All the measured unit cell parameters from AFM image were consistent and in complete agreement with the results of the X-ray diffraction. The microscopic structures of corrugated surface tellurium sheets were strongly affected by the modification of metal double zig-zag chains underneath Te surface. Large difference in the height amplitudes of AFM images in $TaTe_2$ and $Ta_{0.5}V_{0.5}Te_2$ phases was observed and this reflects large difference in the surface electron densities of two phases. On surface, the shorter intralayer Te···Te contacts in $TaTe_2$ induce more electron transfer from Te p-block bands to Ta d-block bands, thus electron density on surface observed in $TaTe_2$ is much lower than that of $Ta_{0.5}V_{0.5}Te_2$. However, in bulk, interlayer Te···Te contacts in V substituted phase are shorter than those in $TaTe_2$ phase, thus tellurium-to-metal electron transfer occurs more easily in $Ta_{0.5}V_{0.5}Te_2$ phase.

Introduction

One of the major research goals in solid state chemistry is understanding the interrelationship between the crystal structure and the physical properties. This understanding is essential because it will lead the way to the rational design and the preparation of new solid materials in a predictable manner.

Since localized defects and structural disorder often lead to some useful changes (metallic to insulating, paramagnetic to ferromagnetic or antiferromagnetic, even nonsuperconducting to superconducting), it is especially important to understand the microscopic local structure. However, detailed atomic scale phenomena in phase transition, structural modulation by chemical substitution or physical modification can not be completely understood using conventional diffraction method and electronic measurments.

Recently, SPM (Scanning Probe Microscopy) techniques including STM (Scanning Tunnelling Microscopy) and AFM (Atomic Force Microscopy) have been applied to examine the surfaces of various solid materials.[1-12] Among many interesting solid state materials, transition metal dichalcogenides are attractive for STM and AFM study because of several advantages their surfaces have. That is, individual layer of these compounds is held by weak van der Waals interactions, therefore, fresh flat surfaces are obtained via relatively easy cleavage and consequent surface deformation is negligible in contrast to the surface of three-dimensional covalent solids.

Commonly, transition metal dichalcogenides 1T-MX_2 (M = transition metal, X = S, Se, Te) adopt CdI_2-type structure and this structure consists of edge sharing MX_6 octahedra.[13] However, MX_2-type layers with different d-electrons exhibit various metal atom clustering with concomitant formation of metal-metal bonds as shown in Figure 1(a)-(e). For example, 1T-TiS_2 phase with d^0 electron count has undistorted hexagonal lattice as shown in Figure 1(a). 1T-MX_2 (M = Ta, X = S, Se) system with d^1 ions exhibits $\sqrt{13}\times\sqrt{13}$ metal atom clustering as shown in Figure 1(e). During the last two decades, a number of theoretical studies have been carried out to explain these structural modulations.[14,15] Among

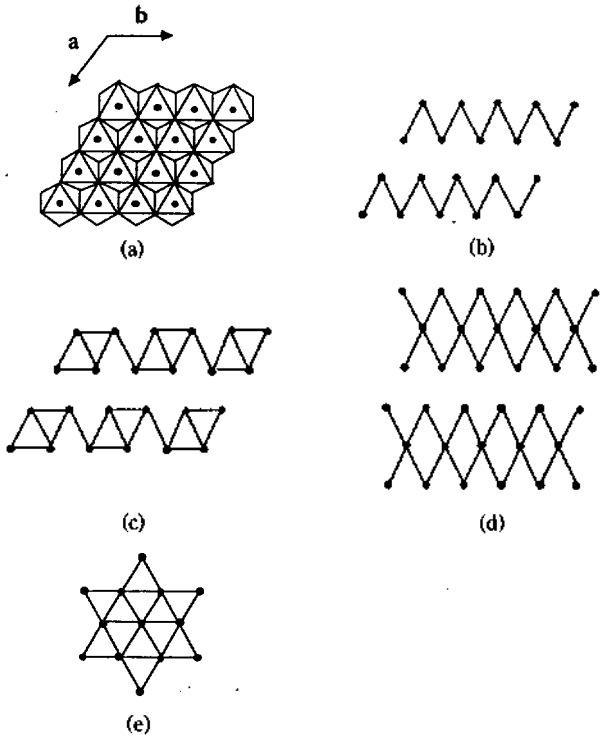

Figure 1. (a) Schematic projection view of an undistorted 1T-TiS_2 layer (ideal CdI_2-structure). (b) Zigzag-chain clustering of metal atoms in 1T-WTe_2 with d^2 ions. (c) Diamond-chain clustering of metal atoms in 1T-ReS_2 with d^3 ions (d) Double zigzag-chain clustering of metal atoms in 1T-$TaTe_2$ with $d^{4/3}$ ions. (e) $\sqrt{13}\times\sqrt{13}$ clustering of metal atoms in 1T-TaS_2 with d^1 ions.

†To whom correspondence be addressed.

them, a mechanism for structural modulation relating charge density wave (CDW) has been proposed by Wilson *et al.* and Mahajan *et al.*[16-18]

Different from 1T-MX_2 (X=S, Se) system, layered transition-metal ditellurides (1T-MX_2, X=Te) frequently have shorter interlayer Te···Te contacts than the van der Waals radii sum due to large covalency of Te. The presence of short Te···Te contacts and their role in controlling structures and physical properties of these tellurides have been recognized in a number of recent studies.[19-22] Incommensurate and commensurate structures have been observed in 1T-MTe_2. Recently, the concept of hidden Fermi surface nesting was proposed to explain the structural modulation of 1T-$TaTe_2$ layers.[14] However, there has been no systematic evaluation of how the structure and the physical properties of these compounds could be effected by their Te···Te contacts.

In the present study, we conducted AFM investigation on $TaTe_2$ surface and examined local structural modification in V substituted $Ta_{1-x}V_xTe_2$ phase in order to understand the structural nature of these materials. The averaged structural changes were studied using a X-ray diffraction technique and the results were compared with the real structural features obtained through AFM images.

Experimental

Single crystals of $TaTe_2$ and $Ta_{1-x}V_xTe_2$ were prepared by chemical vapor transport reaction. Mixtures of Ta(or Nb, V) and Te were sealed in a quartz tube with a trace of I_2 under vacuum. Crystals were grown by heating the mixture at 800 ℃ with 50-100 ℃ gradient for 2-3 weeks. Crystals were obtained at the lower temperature zone.

X-ray measurements were taken at room temperature using a Siemens X-ray diffractometer and Cu Kα radiation. Diffraction data were analyzed using Rietveld-type full-profile refinement technique with a measuring step of 0.02° (in 2θ).

The AFM system used in this study was commercially available AutoProbe LS SPM (Park Scientific Instruments, Sunnyvale CA) equipped with a 5 μm scanner and it was calibrated using mica at ambient condition. The cantilevers were Microlevers (Park Scientific Instruments) of force constant of 0.6 N/m and the scan rates were generally 12.5 Hz or 25 Hz with "height mode". All the samples for AFM experiments were prepared by cleaving the crystals just before the experiments. Single crystals with dimensions of 2×2×0.2 mm were used and the crystal surface images corresponding to crystallographic ab plane were recorded. Measurements and image processing were performed using available software in AutoProbe computer. In several cases, images were filtered with the fast Fourier-transform (FFT) procedure.

Results and Discussion

X-ray diffraction study. The products of $TaTe_2$, $Ta_{1-x}Nb_xTe_2$ and $Ta_{1-x}V_xTe_2$ ($x=0.5$) were black crystals with metallic luster. The powder patterns of these three phases were similar except for the slightly different relative peak intensities and slight shifts in peak positions, which indicates that Ta atoms are substituted by Nb or V atoms without structural change. No extra peaks except the calculated pattern were found. The powder X-ray diffraction patterns were refined with Rietveld-type full-profile refinement technique. The refined parameters used were scale factor, zero point, background parameters, cell parameters, atomic positions and occupancies (Figure 2, Table 1). The refined occupancies suggested that Ta atoms were randomly substituted by V atoms (or Nb atoms) and the resulting composition was $Ta_{0.5}V_{0.5}Te_2$.

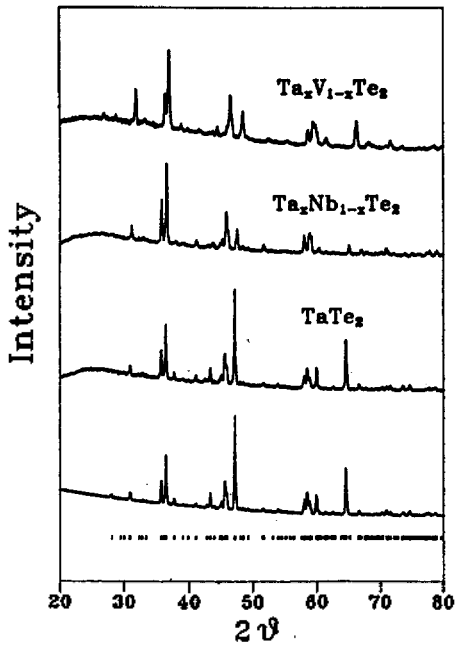

Figure 2. Results of Rietveld refinements for three phases. The fourth pattern from the top represents the calculated data for $TaTe_2$ and the vertical strokes mark the positions of calculated Bragg reflections. R_{wp} values for $TaTe_2$, $Ta_{1-x}V_xTe_2$ and $Ta_{1-x}Nb_xTe_2$ were 7.14%, 7.19% and 3.35% respectively.

Table 1. Refined Parameters for $Ta_{1-x}Nb_xTe_2$ in Monoclinic C2/m Unit Cell

Atom	Position (x, y, z)	Occupancy (%)
Ta1 (2a)	0, 0, 0	50
Nb1 (2a)	0, 0, 0	50
Ta2 (4i)	0.6426 (5), 0, 0.9892 (5)	50
Nb2 (4i)	0.6426 (5), 0, 0.9892 (5)	50
Te1 (4i)	0.6474 (5), 0, 0.2855 (8)	100
Te2 (4i)	0.2935 (4), 0, 0.2127 (7)	100
Te3 (4i)	0.9976 (4), 0, 0.3008 (7)	100

$R_p=2.60\%$, $R_{wp}=3.35\%$.

The results of X-ray diffraction analysis showed that the cell parameters of unit cell decrease when Ta cations of $TaTe_2$ were substituted by V cations (Table 2). The decrease in cell parameters seems to be due to the smaller radius of substituted cations. The solid solutions of three different compositions between $x=0.25$ and 0.5 were examined and they showed continuous structural behavior.

$TaTe_2$ has CdI_2-type structure at high temperature (~800 K) and this structure is distorted to form a double zigzag chains cooling to room temperature.[13a] CdI_2-type transition-

Table 2. Refined Parameters for $Ta_{1-x}V_xTe_2$ in monoclinic C2/m Unit Cell

Atom	Position (x, y, z)	Occupancy (%)
Ta1 (2a)	0, 0, 0	50
V1 (2a)	0, 0, 0	50
Ta2 (4i)	0.6403 (5), 0, 0.9931 (9)	50
V2 (4i)	0.6403 (5), 0, 0.9931 (9)	50
Te1 (4i)	0.6467 (7), 0, 0.2765 (9)	100
Te2 (4i)	0.2955 (6), 0, 0.2222 (8)	100
Te3 (4i)	0.9932 (6), 0, 0.2925 (8)	100

R_p=5.53%, R_{wp}=7.19%.

Table 3. Bond Distances for MX_2 (Å)

Atom 1	Atom 2	$TaTe_2$	$Ta_{0.5}Nb_{0.5}Te_2$	$Ta_{0.5}V_{0.5}Te_2$
(M-M distances)				
M(1)	M(2)(4)	3.351	3.359	3.283
M(2)	M(2)	4.391	4.401	4.501
(M-X distances in centric octahedron)				
M(1)	X(1)(4)	2.801	2.810	2.768
M(1)	X(3)(2)	2.829	2.840	2.789
(M-X distances in acentric octahedron)				
M(2)	X(1)(1)	2.705	2.702	2.529
M(2)	X(2)(2)	2.812	2.765	2.794
M(2)	X(2)(1)	2.832	2.886	2.981
M(2)	X(3)(2)	2.757	2.777	2.709
(X-X distances parallel to layering)				
X(1)	X(2)	3.834	3.796	3.700
X(2)	X(3)	3.806	3.870	3.826
X(1)	X(3)	3.490	3.503	3.548
(X-X distances between layers)				
X(1)	X(1)	3.623	3.584	3.619
X(1)	X(2)	4.009	3.970	3.928
X(2)	X(3)	3.819	3.817	3.786
X(3)	X(3)	3.684	3.654	3.650

metal ditellurides have layers of composition MTe_2, which consists of MTe_6 octahedra by sharing their edges (Figure 1(a)). In each MTe_2 a layer of metal atoms is sandwiched between two layers of tellurium atoms, and the metal atoms of an undistorted MTe_2 layer form a hexagonal lattice. All the Ta-Ta distances are identical in high temperature phase and the Ta-Ta bonds become asymmetric in distorted phase at lower temperature. Consequently, the lattice is distorted from a hexagonal (a_h=3.6351 Å) to a monoclinic superlattice with $c_m \approx 3\sqrt{3}a_h$, $b_m \approx a_h$, $c_m \approx c_h \sin\beta$, $tg(\pi-\beta) \approx c_h/(\sqrt{3}a_h)$.

Table 3 represents important atomic distances obtained from the Rietveld analysis. The observed shortest Ta(1)-Ta (2) distance was 3.35 Å, while the separation between Ta atoms of neighboring chains was 4.39 Å (Ta(2)-Ta(2)), suggesting the distortion was considerable. In the distorted structure, two thirds of Ta(Ta2) atoms deviated from the center and one third of Ta(Ta1) atoms remained in the center of the Te octahedron. The two crystallographically different Ta atoms forming double zigzag chains are emphasized and the resulting monoclinic superstructure is indicated by the dotted lines in Figure 3. It is apparent that the tellurium sheets are distorted in response to the deviation of Ta atoms from the center of octahedron. Figure 4 shows projection view of (010) plane, which illustrates the corrugation of single tellurium-tantalum-tellurium layer. The corrugation pattern is such that, where the metal-metal distances are short, the Te-Te distances in the transverse direction to the layers are lengthened, and vice versa. The tellurium surface thus appears as a series of troughs and crests with a period of $a/2$.

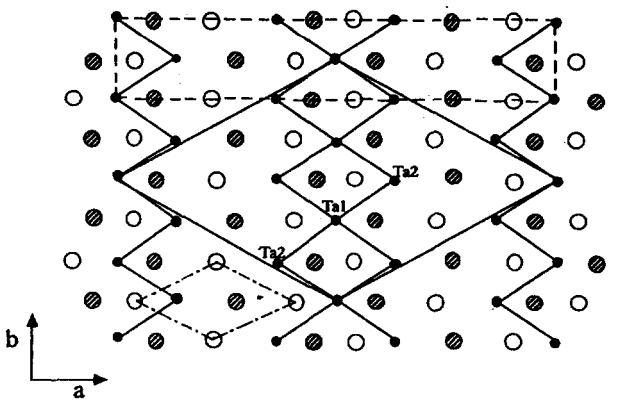

Figure 3. Projection of a single MTe_2 (M=Ta, Nb, V) layer on (001) face in a direction perpendicular to (001). Closed circles are metal atoms. Open circles are tellurium atoms above, and the hatched circles are tellurium atoms below the metal atom sheet, respectively. The shortened metal-metal distances are emphasized by solid lines. The cell of the monoclinic superstructure is indicated by dotted lines and hexagonal superstructure with $a=3a_h$ (where a_h is unit cell parameter of CdI_2-type structure) is indicated by solid lines. Pseudohexagonal subcell (ideal CdI_2-type structure) is indicated by broken lines.

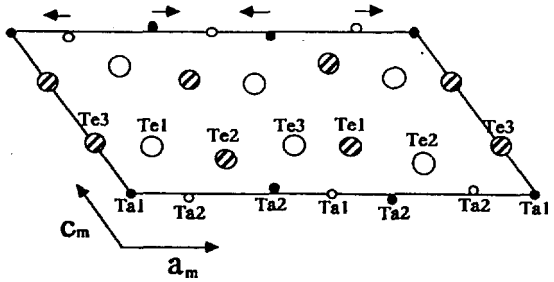

Figure 4. Projection of MTe_2 (M=Ta, Nb, V) structure onto (010) face. Large open circles are tellurium atoms at $y=1/2$, hatched circles are tellurium atoms at $y=0$. Small open circles are metal atoms at $y=1/2$ and closed circles are metal atoms at $y=0$. The directions of displacements of the M(2) atoms from their positions in the CdI_2-type structure are indicated by arrows.

The results of X-ray diffraction analysis for $Ta_{1-x}Nb_xTe_2$ and $Ta_{1-x}V_xTe_2$ phase indicated that V or Nb atoms are randomly distributed on Ta(1) and Ta(2) sites. Since the results are similar in two solid solutions, only $Ta_{1-x}V_xTe_2$ phase will be discussed hereafter. The metal-metal(M-M) bonds in V substituted phase have more asymmetric character than

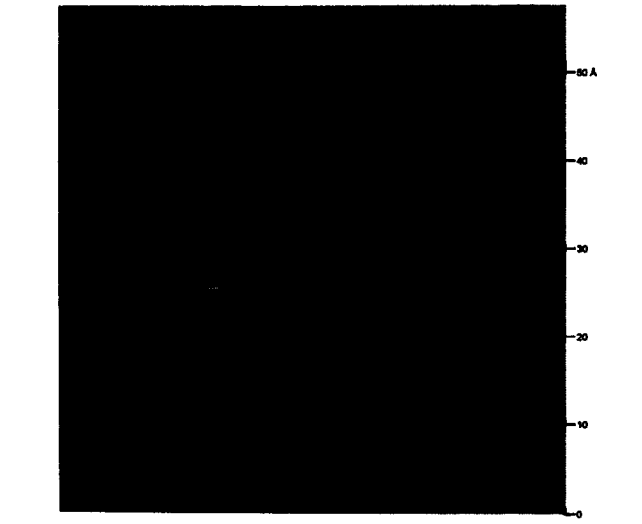

(a)

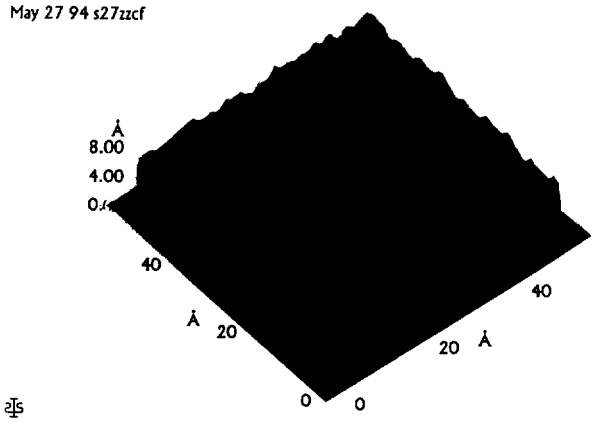

(b)

Figure 5. The AFM image of (001) surface of $TaTe_2$ (a) Two-dimensional surface image and height profile of Te surface of $TaTe_2$. Lower left part of the image is shown after FFT filtering. Triple raws of spots are repeated uniformly. Two brighter rows and one darker row represent higher and lower height atomic row of Te. The height profile of the surface corrugation along the direction of hexagonal superlattice a (the line marked in AFM image) is shown at the lower part of (a). (b) three dimensional surface image of $TaTe_2$.

those in $TaTe_2$ phase, *i.e.*, M(1)-M(2)=3.28 Å and M(2)-M(2) =4.50 Å (where M represents solid solution of Ta and V in $Ta_{1-x}V_xTe_2$).

The shorter M-M distance in V substituted solid solution is rationalized by following arguments. The double metal zigzag chains are formed to stabilize the crystal structure by gaining electronic energy.[14] The reason why the metal-metal bonds in solid solution phase are shorter, thus have more asymmetric character seems to be due to less electron polarizability of the substituted V atoms comparing Ta atoms. Generally, although it is not invariable, 4*d* or 5*d* metal-metal bond has more overlaps than 3*d* bond, thus the 3*d* electron in V substituted phase is more localized. In elemental Ta, the first and second shortest metal bonds are 3.30 and 2.86 Å and those of elemental V are 3.03 and 2.62 Å, respectively. The lower-row metal has more extended d-orbitals, thus the onset distance for metal-metal bonding for their metal clustering is longer than that of the higher-row metal. The observed Ta-Ta distance in $TaTe_2$ phase and M-M distance in $Ta_{1-x}V_xTe_2$ were 3.35 and 3.28 Å, respectively.

AFM study. Compared to the conventional diffraction study, the AFM image can provide highly resolved information of the microscopic structural differences between the pure and the solid solution phase. In the contact mode of AFM, a surface profile is examined by probing the repulsive interatomic force between the tip and surface atoms. Since the replusive force the tip feels at a given location is proportional to the total electron density of the surface, $\rho(r_0)$, AFM images reflect the periodic arrangement of atoms on the surface.

The AFM image of (001) surface of $TaTe_2$ shows repeated triple rows of spots representing the protruded surfaces, in which two bright rows and one dim row represent higher and lower height atomic rows of Te (Figure 5(a)), respectively. Two brighter rows represent Te(3) and Te(1) atoms and one dim row represents Te(2) atoms of Figure 4. The repeating distances of the brightest central row were also regular in $Ta_{1-x}V_xTe_2$ (Figure 6(a)), but the two sides of the central row have different contrast from the image of $TaTe_2$ phase obtained. In the image of $Ta_{1-x}V_xTe_2$, central row among the triple rows was the brightest and two side rows were less bright. The row of brightest spots represents Te(3) and two side rows represent Te(2) and Te(1). The relatively different contrast seems to be due to the different height of metals in the second layer, i.e., the height of M(2)-M(1) underneath Te(3) is higher than that of M(2)-M(1) underneath Te(1). However, such effect from second metal layer is not significant in $TaTe_2$ phase because metal-metal distances are longer than those in $Ta_{1-x}V_xTe_2$ phase.

All the measured unit cell parameters of commensurate superlattice from the AFM images are consistent and in complete agreement with the results of X-ray diffraction study. The distance between spots in $TaTe_2$ image within a row, 3.6± 0.2 Å, corresponds to the monoclinic unit cell parameter b, and the periodic distance in the perpendicular direction to the row, 19.2± 0.5 Å, corresponds to the unit cell parameter a (Figure 5(a)).

Figures 5(b) and 6(b) show the three-dimensional surface images and the height profiles of Te surface of $TaTe_2$ and $Ta_{1-x}V_xTe_2$. The main features of the images remained the same (*i.e.* grouping of three rows), and the periodicity of the intensity corresponds to the monoclinic cell parameters. However, the overall amplitude of these corrugations in V doped phase was much greater than that of pure phase, *i.e.*, their amplitudes are ~5 Å and ~2 Å, respectively. Those different surface features are the first time to be observed and those will significantly affect surface reactivity. On the basis of the crystal structure, the largest differences between Te(2) and Te(3) along the perpendicular direction to the layer are only 0.56 and 0.46 Å in $TaTe_2$ and $Ta_{1-x}V_xTe_2$ phases,

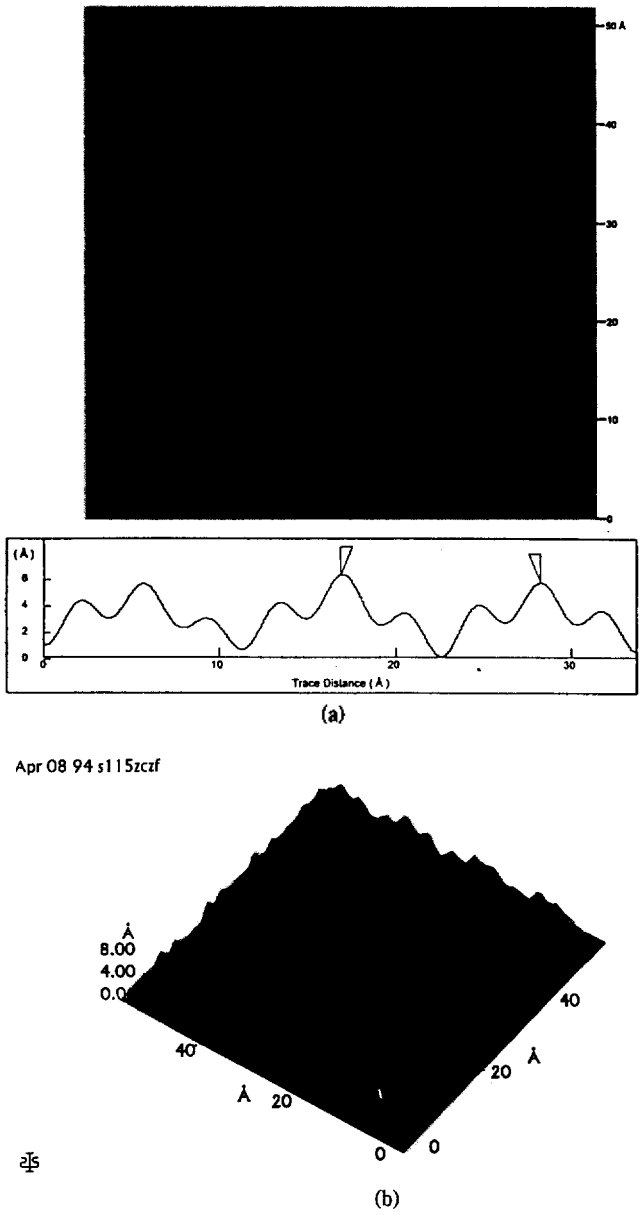

Figure 6. (a), (b). Two- and three-dimensional surface image and height profile of Te surface of $Ta_{1-x}V_xTe_2$. Lower left part of the image is shown after FFT filtering. The hieght profile of the surface corrugation along the direction of hexagonal superlattice a is shown at the lower part of (a). The unit cell of monoclinic superstructure is indicated in (a).

respectively, and the lattice parameter c for the $Ta_{0.5}V_{0.5}Te_2$ is only 1.3% smaller than that of the $TaTe_2$ phase. Since the height difference between the maximum and minimum amplitude was 0.94 and ~2 Å in AFM image of $TaTe_2$ and $Ta_{1-x}V_xTe_2$ phases, respectively, the pure geometric factors cannot account for such a large surface height difference observed.

It has been known that, for layered solids, structural and electronical properties of the surface are usually similar to those of the bulk. In many low-dimensional transition metal disulfides and diselenides, the similarity of the bulk and the surface is due to low free energy of the van der Waals planes. However, layered transition-metal ditellurides frequently have shorter interlayer Te···Te contacts than the van der Waals radii sum due to more covalency of Te. In transition metal tellurides, the oxidation state is given by $Ta^{4+}(X^{2-})_2$. The tellurium p-band is completely filled, thus top portion of the p-band has antibonding character. When Te···Te contacts are shortened, the p-antibonding band energy is raised so that significant overlap with the bottom portion of metal d-band is possible. The short distance in interlayer Te···Te contacts is an indication of electron transfer.

It has been reported that their d-electron count is actually close to $d^{4/3}$ instead of d^1 for 1T-MTe_2 (M=V, Nb, Ta) systems due to the partial tellurium to metal electron transfer.[20(a)] The 1T-MTe_2(M=V, Nb, Ta) system with 4/3 d-electron has their metal ions clustered into "double zigzag-chains" as mentioned in the introduction section. For this $p \rightarrow d$ electron transfer, its interlayer Te···Te contacts play a key role because the overlap between the p_z-orbitals associated with the interlayer Te···Te contacts is most effective in raising the top portion of the Te p-block bands. As a consequence, the layered transition metal ditellurides are likely to possess a three dimensional metallic character and a slight change in their interlayer contact significantly affects their structural and physical properties. The shorter interlayer Te···Te contacts than those of $TaTe_2$ phase are observed in solid solution phase, thus more $p \rightarrow d$ electron transfers are possible in the bulk sample.

However, the interlayer Te···Te contacts are not present on the surface. Thus, when the microscopic structures of surface are considered, it is necessary to examine how this electron transfer is affected by the intralayer Te···Te contacts. Both the X-ray diffraction analysis and AFM image analysis show that the Te···Te distance within a layer in $TaTe_2$ phase (Te(1)-Te(3)=3.49 Å) is shorter than that in V doped phase (Te(1)-Te(3)=3.55 Å). This shortened intralayer Te··· Te contact will raise the energy level of Te p-block bands. Consequently, electrons can easily be transferred to the bottom of Ta d-block bands. Therefore, lower amplitude of the protrusion illustrated in AFM image (Figure 7) of pure $TaTe_2$ phase reflects the lower electron density on Te p-block bands.

Conclusions

Our study reveals that the bright spots in AFM images of $TaTe_2$ and $Ta_{0.5}V_{0.5}Te_2$ are associated with the surface topography of the tellurium atoms. The different contrast on AFM image reflects that the metal-metal (M-M) bondings in V substituted phase have more asymmetric character than those of undoped $TaTe_2$. The surprisingly large difference in the height amplitudes of AFM images in two phases suggests the difference in electron density of the surface Te atoms. The shorter intralayer Te···Te contacts in $TaTe_2$ phase induce more electron transfer from Te p-block bands to Ta d-block bands, thus electron density of the surface Te is much lower than that of $Ta_{0.5}V_{0.5}Te_2$. However, in bulk, interlayer Te···Te contacts in V substituted phase are shorter than those of $TaTe_2$ phase due to the small atomic radius of V and this dominantly affects on the electron trnasfer.

Acknowledgment. The present studies were supported by the Basic Science Research Institute Program, Ministry

of Education, BSRI-94-3413 and in part by the Korean Science and Engineering Foundation (92-25-00-02). ICJ acknowledges financial support in part from the Korean Science and Engineering foundation (90-03-00-03).

References

1. Wiesendanger, R.; Güntherodt, H. J. Eds. *Scanning Tunneling Microscopy*; Springer-Verleg: Heidelberg, 1992; Vols. I, II.
2. Behm, J.; Garcia, N. Rohrer, H. Eds. *Scanning Tuneling Microscopy and Related techniques*; Kluwer Academic Publishers: Dordrecht, The Netherlands, 1990.
3. Wu, X. L.; Lieber, C. M. *J. Am. Chem. Soc.* **1989**, *111*, 2731.
4. Kelty, S. P.; Lieber, C. M. *J. Phys. Chem.* **1989**, *93*, 5983.
5. Lieber, C. M.; Wu, X. L. *Acc. Chem. Res.* **1991**, *24*, 170.
6. Chen, H.; Wu, X. L.; Lieber, C. M. *J. Am. Chem. Soc.* **1990**, *112*, 3326.
7. Sakamaki, K.; Fujishima, A.; Onuki, Y. *J. Phys. Chem. Solid* **1991**, *52*, 409.
8. Ren, J.; Whangbo, M. H. *J. Phys. Chem.* **1993**, *97*, 4764.
9. Ren, J.; Whangbo, M. H.; Bengel, H.; Cantow, H. J.; Magonov, S. N. *Chem. Mater.* **1993**, *5*, 1018.
10. Whangbo, M. H.; Ren, J.; Canadell, E.; Louder, D.; Parkinson, B. A.; Bengel, H.; Magonov, S. N. *J. Am. Chem. Soc.* **1993**, *115*, 3760.
11. Parkinson, B. A.; Ren, J.; Whangbo, M. H. *J. Am. Chem. Soc.* **1991**, 113, 7833.
12. Magonov, S. N.; Zönchen, P.; Rotter, H.; Cantow, H. J.; Thiele, G.; Ren, J.; Whangbo, M. H. *J. Am. Chem. Soc.* **1993**, *115*, 2495.
13. (a) Hulliger, F. *Structural Chemistry of Layer-Type Phase*; Levy, F. Ed.; D. Reidel Publishing Co: Dordrecht-Holland, 1976. (b) Ghorayeb, A. M.; Liang, W. Y.; Toffe, A. D. *Intercalation in Layered Materials*; Dresselhaus, M. S. Ed.; Plenum Press: New York, 1986; p 135.
14. (a) Whangbo, M. H.; Canadell, E. *J. Am. Chem. Soc.* **1992**, *114*, 9587. (b) Whangbo, M. H.; Canadell, E.; Foury, P.; Pouget, J. P. *Science* **1991**, *252*, 96.
15. Rovira, C.; Whangbo, M. H. *Inorg. Chem.* **1993**, *32*, 4094.
16. Wilson, J. A.; Disalvo, F. J.; Mahajan *Advances in Physics* **1975**, *24*, 117.
17. Williams, P. M.; Parry, G. S.; Scruby, C. B. *Phil. Mag.* **1974**, *29*, 695.
18. Thompson, A. H. *Phys. Rev. Lett.* **1975**, *34*, 520.
19. (a) Brown, B. E. *Acta Cryst.* **1966**, *20*, 264. (b) Bronsema, K. D.; Bus, G. W.; Wiegers *J. Solid State Chem.* **1984**, *53*, 415.
20. (a) Canadell, E.; Jobic, S.; Brec, R.; Rouxel, J.; Whangbo, M. H. *J. Solid State Chem.* **1992**, *99*, 189. (b) Revolinsky, E.; Brown, B. E.; Beerntsen, D. J.; Armitage, C. H. *J. Less-Common Met.* **1965**, *8*, 63.
21. Jobic, S.; Brec, R.; Rouxel, J. *J. Solid State Chem.* **1992**, *96*, 169.
22. Mar, A.; Jobic, S.; Ibers, J. A. *J. Am. Chem. Soc.* **1992**, *114*, 8963.

Interaction of Hydrosilanes with the Surface of Rhodium

Bong Hyun Boo*, Seung Ki Hong, Sun Sook Lee, and Hyun Sook Kim

**Department of Chemistry, Chungnam National University, Taejon 305-764, Korea*
Center for Molecular Science, 373-1 Kusung-dong Yusung-gu, Taejon 305-701, Korea
Received August 26, 1994

Interaction of triethylsilane and diphenylsilane (Ph_2SiH_2, Ph_2SiD_2) with the surfaces of rhodium has been examined by trapping the reaction intermediates with 2,3-dimethyl-1,-3-butadiene. 1,4-Hydrosilylation of the diene is predominantly observed to occur under mild condition over the rhodium catalyst. It is inferred from the product analyses that silylene and silyl radicals bonded to rhodium surfaces are the intermediates for addition of silylene to the diene, and for 1,4-hydrosilylation, respectively.

Introduction

Transition metal complexes containing silyl radicals or silylenes as ligands are relatively uncommon; however, some of those complexes have been isolated as stable compounds.[1,2] Also a recent ion beam study of the reactions of transition metal ions with various silanes in the gas phase is quite informative as to detailed mechanistic interpretation of transition metal-catalyzed hydrosilylation and provides estimates of bond energies of transition metal-silylenes.[3] There are numerous reports on the hydrosilylations of olefin and diene catalyzed by transition metals and their complexes.[4-9] Activation of Si-H bonds by transition metal is presumed to play an important role in the catalytic hydrosilylation, and direct evidence for this oxidative addition is shown by spectroscopy at low temperatures.[10,11]

We are concerned about the formation of silyl radicals and silylenes bonded to transition metal under mild reaction condition. Much endeavor has also been made for obtaining the mechanistic information about the behaviors of silylhyd-